The University of Osaka
Institutional Knowledge Archive

Title	Equilibrium thermodynamic theory for the evaluation of temperature distributions in overdriven steady-plane wave fronts
Author(s)	Sano, Tomokazu; Sano, Yukio
Citation	Journal of Applied Physics. 2001, 90(8), p. 3754-3761
Version Type	VoR
URL	https://hdl.handle.net/11094/89431
rights	This article may be downloaded for personal use only. Any other use requires prior permission of the author and AIP Publishing. This article appeared in Sano T., Sano Y. Equilibrium thermodynamic theory for the evaluation of temperature distributions in overdriven steady-plane wave fronts. Journal of Applied Physics, 90, 8, 3754 and may be found at https://doi.org/10.1063/1.1397278.
Note	

Equilibrium thermodynamic theory for the evaluation of temperature distributions in overdriven steady-plane wave fronts

Tomokazu Sano and Yukio Sano

View Online   Export Citation

ARTICLES YOU MAY BE INTERESTED IN

Journal of Applied Physics

Equilibrium thermodynamic theory for the evaluation of temperature distributions in overdriven steady-plane wave fronts

Tomokazu Sano[a)]
Graduate School of Engineering, Osaka University, Suita, Osaka 565-0871, Japan

Yukio Sano
Kobe University of Mercantile Marine, Higashi-Nada-Ku, Kobe 658-0022, Japan

Temperature distributions in overdriven steady wave fronts in solid 2024 Al shocked up to 80 GPa, in which no melting occurred in the wave fronts, were evaluated using the equilibrium thermodynamic theory. The effective strain increments were sufficiently small and the effective temperature rise times were sufficiently long with respect to electron–phonon relaxation times to justify using equilibrium thermodynamics. In addition, the sufficiently large viscous-stress components supported the efficacy of the thermodynamic theory. The same is true of shocks up to 250 GPa in solid Pt and 230 GPa in solid Fe. Furthermore, the influence of viscous stress was examined by evaluating the temperature distributions for inviscid 2024 Al, Pt, and Fe solids using the equations for temperature derived from the Mie–Grüneisen equation. Finally, we demonstrate that there might be a solid–liquid–solid Hugoniot between the solid and liquid–solid Hugoniots for Fe and estimate the solid–liquid–solid and liquid–solid Hugoniots. © *2001 American Institute of Physics.* [DOI: 10.1063/1.1397278]

I. INTRODUCTION

Sano and Abe[1] developed the inside temperature (IT_{IM}) method, which implicitly includes heat transport, to estimate temperature distributions in steady wave fronts in a solid. In this method, there is a fundamental assumption that the state of the solid in the wave front is close to thermodynamic equilibrium. In addition, there is an assumption that heat transport cancels the work performed by thermal stress in the region of the wave front so both can be neglected. This assumption of heat transport is valid if the viscous component of normal stress is sufficiently large compared with its thermal component. Sano and Abe evaluated the temperature distributions in multiple-structure waves and overdriven shock waves for shocks up to 140 GPa in yttria-doped tetragonal zirconia. The evaluated temperatures behind the shocks were sufficiently correct as compared with those obtained using the Walsh–Christian (WC) theory[2] or the shock temperature method. The evaluated distributions were fairly correct because the viscous-stress component was sufficiently large. Therefore, the fundamental assumption and the assumption of heat transport used in the IT_{IM} method were considered valid and, as a result, this method was deemed effective. The main purpose of the present study is to present a method for calculating the temperature in shock fronts that have a physically reasonable variation of temperature through the shock front, namely, an essentially linear variation of temperature versus volume. This method is appropriate for temperature distributions in the shock front for shocks up to 200–300 GPa in metals. The subsidiary purposes are (1) to examine

the validity of equilibrium thermodynamics for the temperature calculations, and (2) to look for intermediate states of melting in shock fronts.

Strain rates inside overdriven shock wave fronts induced by 200–300 GPa shocks might reach 10^{11}–10^{12} s^{-1}. The deformation at any material point in the wave front does not change greatly during electron–phonon relaxation times of 10^{-14}–10^{-13} s, which are dominant up to 200–300 GPa. The homogeneous volumetric component of deformation is even smaller because plastic flow, which is heterogeneous on an atomic scale, is very large. Consequently, if the temporal rates of change of the inside temperatures are slow compared with the characteristic relaxation rates of temperature, then the electron–phonon system can maintain itself near mechanical and thermal equilibrium for shocks up to 200–300 GPa. The homogeneous component supports a great part of the stress on the Rayleigh line, which is used in thermodynamics of irreversible processes. Therefore, irreversible thermodynamics is applicable to overdriven shocks up to 200–300 GPa if strain rates are smaller than 10^{12} s^{-1} and if the state inside the shock wave front structure can be regarded as being essentially at thermal equilibrium.

It is not known, however, whether irreversible thermodynamics is a valid theory for overdriven shocks because the thermodynamic equilibrium of the states has not yet been determined. This equation is still open because macroscopic treatment of a material process without thermodynamics is conceptually difficult.[3] One method to answer this question is to verify that the system remains near thermodynamic equilibrium throughout the shock process, namely that the fundamental assumption is valid. This can be verified by first calculating the process from irreversible thermodynamics

---
[a)]Electronic mail: sano@mapse.eng.osaka-u.ac.jp

and then comparing the temporal rates of change with appropriate characteristic rates as described above.

In the present study, the validity of the fundamental assumption for metals in a range of temperatures below their melting points, namely, for shocks up to 80 GPa in 2024 Al,[4] 250 GPa in Pt,[4] and 230 GPa in Fe,[5] was examined by estimating effective strain rates and temperature rise times using the equilibrium thermodynamic theory (IT_{IM} method). In addition, the efficacy of this method was verified by the sufficiently large viscous-stress components compared with the thermal component evaluated for those shocks. Furthermore, the influence of viscous stress was examined by evaluating the temperature distributions in overdriven steady wave fronts in an inviscid 2024 Al solid shocked up to 80 GPa using an equation for temperature derived from the Mie–Grüneisen equation and comparing with those evaluated using the IT_{IM} method. Here, an inviscid solid means a solid in which no viscous stress is induced during shock loading. The influence of viscous stress was also examined for shocks up to 250 GPa in Pt and 230 GPa in Fe. Finally, intermediate states of melting in shock fronts were investigated in Fe.

II. EQUILIBRIUM THERMODYNAMIC THEORY

The IT_{IM} method is first described. This method provides adequate treatment of the temperature distributions in the shock fronts. Next, a method for estimating effective temperature thicknesses is presented. Finally, equations by which the temperature distributions in inviscid solids can be correctly estimated are derived.

A. IT_{IM} method

Sano and Abe[1] developed the IT_{IM} method for estimating temperature T in a steady wave front in a solid. Normal stress σ in a steady wave front is related to specific volume V by the Rayleigh line equation

$$d\sigma = -\rho_0^2 U_S^2 dV, \qquad (1)$$

where U_S is a constant velocity of the wave front and $\rho = 1/V$ is material density. Subscript 0 refers to a reference state. They derived the following approximate equation by assuming that heat transport and the work performed by the thermal stress could cancel each other out:

$$T\,dS = -(\sigma - \sigma_E)dV, \qquad (2)$$

where S is entropy and σ_E is the thermal component of the normal stress σ. This assumption is valid if the work performed by viscous stress is sufficiently large compared with the work performed by thermal stress and heat transport. The set of equations used in this method consists of an irreversible thermodynamic equation obtained by equating Eq. (2) with the thermodynamic identity, the equation for cold stress σ_C, and the equation for thermoelastic stress σ_E. The thermodynamic equation is expressed by

$$C_V \frac{dT}{dV} + \frac{\gamma_0}{V_0} C_V T = -(\sigma - \sigma_E), \qquad (3)$$

where γ is the Grüneisen parameter, C_V is the heat capacity at a constant volume on the Rayleigh line, and γ/V

$= \gamma_0/V_0$ is assumed. The heat capacities for 2024 Al and Pt are given by the sum of a lattice and an electron part.[6]

$$C_V = 3Nk + \Gamma T, \qquad (4a)$$

where N is the number of atoms per mole, k is the Boltzmann constant, and Γ is given by $\Gamma = \Gamma_0 (V/V_0)^g$. The values of g and Γ_0 for 2024 Al and Pt are listed in Table I. For Fe,[5]

$$C_V = 3Nk. \qquad (4b)$$

The equation for σ_C is given by

$$\sigma_C = \sigma_H - \sigma_{T_H}, \qquad (5)$$

where σ_H is a known Hugoniot function for normal stress, which is represented as $\sigma_H(V)$, and σ_{T_H} is a Hugoniot function for thermal stress, $\sigma_{T_H}(V)$, which is expressed by

$$\sigma_{T_H} = \frac{\gamma_0}{V_0} \int_0^{T_H} C_V\,dT,$$

where T_H is the temperature behind the wave front, namely, the Hugoniot temperature. The equation for σ_E is given by

$$\sigma_E = \sigma_C + \sigma_T, \qquad (6)$$

where σ_T is the thermal stress expressed by

$$\sigma_T = \frac{\gamma_0}{V_0} \int_0^T C_V\,dT.$$

Equations (3)–(6) were analyzed by an iterative method using a known Hugoniot function $\sigma_H(V)$ and a known Rayleigh line-stress function $\sigma(V)$ to determine the temperature, cold compression curve, thermoelastic stress, and viscous stress.

B. Temperatures behind wave fronts

The solution of Eq. (3) is given by

$$T = T_0 e^{(\gamma_0/V_0)(V_0 - V)} - e^{-(\gamma_0/V_0)V}$$

$$\times \int_{V_0}^{V} \frac{1}{C_V} (\sigma - \sigma_E) e^{(\gamma_0/V_0)V} dV.$$

The solution for the temperatures behind the wave fronts T_H is obtained by substituting V_H into V in the above equation.

TABLE I. Input data for shock calculations in 2024 Al[a], Pt[a], and Fe[b].

Quality	2024 Al	Pt	Fe
T_0 (10^3 K)	0.293	0.293	0.293
ρ_0 (g/cm^3)	2.785	21.44	7.85
c (cm/μs)	0.533	0.363	0.3574
s	1.338	1.472	1.920
q (μs/cm)	—	—	−0.68
γ_0	2.05	2.66	1.69
Γ_0 (10^{-4} cal /mole K^2)	3.30	16.4	—
g	1.8	2.28	—
κ (cal/cm s K)	0.48	0.20	0.10

[a]See Ref. 6.
[b]See Ref. 10.

$$T_H = T_0 e^{(\gamma_0/V_0)(V_0-V_H)} - e^{-(\gamma_0/V_0)V_H}$$

$$\times \int_{V_0}^{V_H} \frac{1}{C_V}(\sigma-\sigma_E)e^{(\gamma_0/V_0)V}dV. \tag{7}$$

The left side of the WC equation, which is expressed by Eq. (A7), is calculated using the above solution to become

$$C_{VH}\frac{dT_H}{dV_H} + C_{VH}\frac{\gamma_0}{V_0}T_H$$

$$= -C_{VH}e^{-(\gamma_0/V_0)V_H}\frac{d}{dV_H}\int_{V_0}^{V_H}\frac{1}{C_V}(\sigma-\sigma_E)e^{(\gamma_0/V_0)V}dV. \tag{8}$$

The following equation holds:

$$\frac{d}{dV_H}\int_{V_0}^{V_H}\frac{1}{C_V}(\sigma-\sigma_E)e^{(\gamma_0/V_0)V}dV$$

$$= \left[\frac{d}{dV_H}\int_{V_0}^{V_H}\frac{1}{C_V}(\sigma-\sigma_E)dV\right]e^{(\gamma_0/V_0)V_H}.$$

Consequently, Eq. (8) is reduced to

$$C_{VH}\frac{dT_H}{dV_H} + C_{VH}\frac{\gamma_0}{V_0}T_H = -C_{VH}\frac{d}{dV_H}\int_{V_0}^{V_H}\frac{1}{C_V}(\sigma-\sigma_E)dV. \tag{9}$$

The solution Eq. (7) thus satisfies Eq. (9).

If C_V is constant, then Eq. (9) is reduced to

$$C_{VH}\frac{dT_H}{dV_H} + C_{VH}\frac{\gamma_0}{V_0}T_H = -\frac{d}{dV_H}\int_{V_0}^{V_H}(\sigma-\sigma_E)dV. \tag{10a}$$

If $C_V = 3Nk + \Gamma T$ with $\Gamma T/3Nk \ll 1$, then an approximate equation is obtained from Eq. (9)

$$C_{VH}\frac{dT_H}{dV_H} + C_{VH}\frac{\gamma_0}{V_0}T_H$$

$$= -\left(1+\frac{\Gamma_H T_H}{3Nk}\right)\frac{d}{dV_H}\int_{V_0}^{V_H}(\sigma-\sigma_E)dV. \tag{10b}$$

The right sides of Eqs. (10a) and (10b) are transformed as

$$\frac{d}{dV_H}\int_{V_0}^{V_H}(\sigma_E-\sigma_V)dV$$

$$= -\frac{d}{dV_H}\int_{V_0}^{V_H}(\sigma-\sigma_H)dV + \frac{d}{dV_H}\int_{V_0}^{V_H}(\sigma_E-\sigma_H)dV,$$

where the first term of the right side is the derivative of the crescent area enclosed by a Rayleigh line and the Hugoniot with respect to V_H, which is expressed by[1]

$$-\frac{d}{dV_H}\int_{V_0}^{V_H}(\sigma-\sigma_H)dV = \frac{1}{2}\frac{d\sigma_H}{dV_H}(V_0-V_H) + \frac{1}{2}(\sigma_H-\sigma_0),$$

whereas the second term is zero because

$$-\frac{d}{dV_H}\int_{V_0}^{V_H}(\sigma-\sigma_E)dV = \sigma_E(V_H) - \sigma_H(V_H) = 0.$$

Therefore, Eq. (10a) is of the same form as the WC equation

$$C_{VH}\frac{dT_H}{dV_H} + C_{VH}\frac{\gamma_0}{V_0}T_H = \frac{1}{2}\frac{d\sigma_H}{dV_H}(V_0-V_H) + \frac{1}{2}(\sigma_H-\sigma_0). \tag{11}$$

Thus, the temperatures behind the wave fronts obtained using the IT_{IM} method are consistent with the correct values obtained using the WC equation if C_V is constant. In addition, for shocks up to 200–300 GPa in metals, the IT_{IM} method is a reasonable approximation to the standard method because $\Gamma T/3Nk \ll 1$. Therefore, the IT_{IM} method is expected to estimate the temperature distributions in the wave fronts to a sufficient approximation if the fundamental assumption and the assumption of heat transport are valid.

C. Effective temperature thickness

The effective thickness of the spatial profile of temperature (effective temperature thickness) ΔZ is defined by[6,7]

$$\frac{\Delta T}{\Delta Z} = \left|\frac{dT}{dZ}\right|_{max}, \tag{12}$$

where Z is the Lagrangian coordinate moving with the same velocity as the constant velocity of an overdriven steady wave front, which is of an infinite width,[8] and $\Delta T = T_H - T_0$. The heat flux is thus assumed to vary spatially slowly everywhere in the wave front. In general, the effective temperature thickness is greater than the effective specific-volume thickness.[6] Derivative dT/dZ is related to heat flux $J(Z)$ by the steady heat conduction equation

$$J = -\frac{\kappa}{1-\varepsilon}\frac{dT}{dZ}, \tag{13}$$

where κ is the thermal conductivity and $\varepsilon(Z) = 1 - V(Z)/V_0$ is the strain. Derivative $|dT/dZ|$ is its maximum when $(1-\varepsilon)J$ is maximum, and this yields

$$\Delta Z = \frac{\kappa(T_H-T_0)}{\{(1-\varepsilon)J\}_{max}}. \tag{14}$$

The continuity equation for heat transport is given by

$$\frac{dJ}{dZ} = \rho_0 U_S \frac{dQ}{dV}\frac{dV}{dZ}, \tag{15}$$

where Q is the heat transferred to the material. The specific volume wave in the steady wave front is assumed to extend from $Z=0$ to $Z=\infty$. By integrating both sides of Eq. (15) from 0 to Z and then using $J(0)=J_H=0$, the equation for heat flux is obtained:

$$J = U_S(\varepsilon_H-\varepsilon)\frac{dQ}{dV}, \tag{16}$$

where $\varepsilon_H = 1 - V_H/V_0$.

The quantity $\{(1-\varepsilon)J\}_{max}$ in Eq. (14) is determined by incorporating Eq. (16) into the IT_{IM} method, where it was assumed that $dQ/dV = \sigma_E - \sigma_{S_0}$, where σ_{S_0} is the stress that varies along an isentrope passing through the reference state. The effective temperature thickness is calculated, irrespective of the form and the effective thickness of the specific volume wave.

TABLE II. Effective temperature thicknesses ΔZ obtained using the equilibrium thermodynamic theory, shock wave velocities, and effective temperature rise times Δt for 20, 40, 60, and 80 GPa shocks in 2024 Al, for 100, 150, 200, and 250 GPa shocks in Pt, and for 100, 150, 200, and 230 GPa shocks in Fe.

2024 Al				Pt				Fe			
Shock (GPa)	$\Delta Z \times 10^7$ (m)	U_S (m/s)	$\Delta t \times 10^{11}$ (s)	Shock (GPa)	$\Delta Z \times 10^7$ (m)	U_S (m/s)	$\Delta t \times 10^{11}$ (s)	Shock (GPa)	$\Delta Z \times 10^7$ (m)	U_S (m/s)	$\Delta t \times 10^{11}$ (s)
20	3.602	6753	5.334	100	0.7053	5003	1.410	100	0.2373	6891	0.3444
40	1.495	7795	1.918	150	0.4784	5502	0.8696	150	0.1832	7847	0.2334
60	1.036	8659	1.196	200	0.3719	5941	0.6260	200	0.1547	8643	0.1789
80	0.8334	9409	0.8858	250	0.3079	6338	0.4858	230	0.1429	9068	0.1576

D. Temperature in inviscid solids

A quadratic equation for the temperature in the wave front T is obtained by substituting Eq. (4a) into the equation for σ_T shown above. The solution of this quadratic equation is given by

$$T = \frac{-3Nk + \sqrt{(3Nk)^2 + 2\Gamma(V_0/\gamma_0)\sigma_T}}{\Gamma}, \quad (17a)$$

where $\sigma_T = \sigma_E - \sigma_C$ for an inviscid solid. σ is correctly given by Eq. (1) and σ_C is evaluated correctly using the WC equation. Therefore, Eq. (17a) correctly estimates temperature distributions in the wave fronts in an inviscid solid. On the other hand, for Eq. (4b)

$$T = \frac{1}{3Nk}\frac{V_0}{\gamma_0}\sigma_T. \quad (17b)$$

Equations (17a) and (17b) are used to examine the influence of viscous stress on the temperature distributions.

III. RESULTS

A. Thermodynamic equilibrium

The data used for calculating the shocks in 2024 Al are listed in Table I.[6] The effective temperature thicknesses ΔZ and rise times Δt for 20, 40, 60, and 80 GPa shocks obtained using the equilibrium thermodynamic theory are given in Table II, where $\Delta t = \Delta Z/U_S$. The very small effective temperature thicknesses indicate that there is a region where temperatures change rapidly in each wave front, despite the fact that the heat flux was assumed to vary gradually everywhere spatially. In this region plastic flow, which is heterogeneous on an atomic scale, is very large. Effective strain rates $\dot{\varepsilon}$ calculated by $\dot{\varepsilon} = \varepsilon_H/\Delta t_s$ for 20, 40, 60, and 80 GPa shocks using Hugoniot strain ε_H and $\Delta t_s \cong \Delta t/3$ (see Ref. 6) are listed in Table III. The effective strain rate of approximately 1.1×10^{11} s^{-1}, in which a relatively large plastic-

flow-deformation component was included, was obtained for the 80 GPa shock. Even this large strain rate only yields an increase in strain on the order of 10^{-3} during the electron–phonon relaxation times for metals (on the order of 10^{-14} s), which are dominant at temperatures above the Debye temperature for shocks up to 200–300 GPa. In addition, the temperature rise time of approximately 0.89×10^{-11} s for the 80 GPa shock was sufficiently long compared with the relaxation times. Wallace[9] discussed the question of equilibrium in solid metals in detail. It is clear from Wallace's discussion that the electron–phonon system remains near thermodynamic equilibrium even in the region where temperatures vary rapidly due to the sufficiently small strain increase and long temperature rise times on the relaxation time scale. Therefore, the fundamental assumption is valid in 2024 Al for up to 80 GPa. The data used for calculating the shocks in Pt are listed in Table I. For 100, 150, 200, and 250 GPa shocks, the values of ΔZ and Δt are given in Table II and the values of $\dot{\varepsilon}$ are given in Table III. The fundamental assumption is also valid up to 250 GPa in Pt for the same reason as for 2024 Al. We used the data of McQueen et al.,[10] which are listed in Table I, and $C_V = 3Nk$ as in Ref. 5 for Fe. For 100, 150, 200, and 230 GPa shocks, the values of ΔZ and Δt are given in Table II and the values of $\dot{\varepsilon}$ are given in Table III. The fundamental assumption was also valid up to 230 GPa in Fe.

B. Efficacy of the IT$_{IM}$ method

Figures 1(a)–1(d) show thermoelastic stress distributions for the 20, 40, 60, and 80 GPa shocks in 2024 Al obtained using the IT$_{IM}$ method, together with the Rayleigh line and the Hugoniot curve. These figures demonstrate that the viscous-stress components $\sigma_v = \sigma - \sigma_E$ are sufficiently large compared with the thermal-stress component $\sigma_T = \sigma_E - \sigma_C$. Therefore, the assumption of heat transport was valid for shocks up to 80 GPa. Thus, the temperature distributions in

TABLE III. Hugoniot strains ε_H and effective strain rates $\dot{\varepsilon}$ for 20, 40, 60, and 80 GPa shocks in 2024 Al, for 100, 150, 200, and 250 GPa shocks in Pt, and for 100, 150, 200, and 230 GPa shocks in Fe.

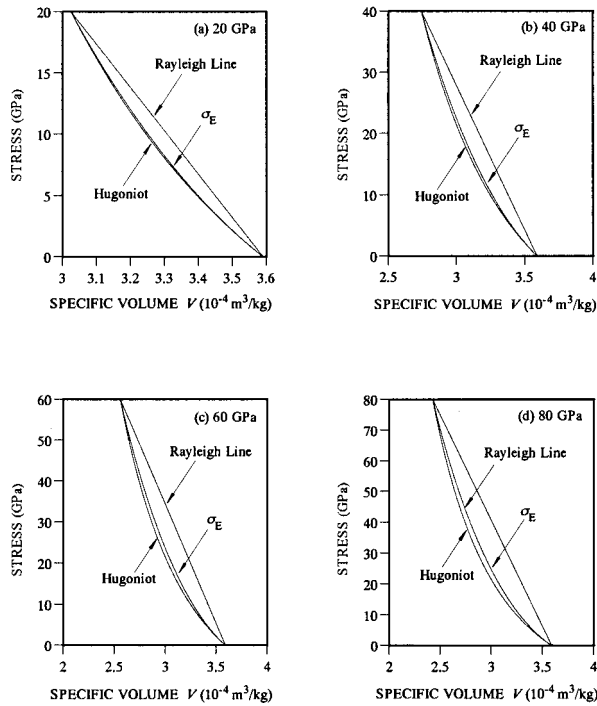| 2024 Al			Pt			Fe		
Shock (GPa)	ε_H	$\dot{\varepsilon} \times 10^{-11}$ (s^{-1})	Shock (GPa)	ε_H	$\dot{\varepsilon} \times 10^{-11}$ (s^{-1})	Shock (GPa)	ε_H	$\dot{\varepsilon} \times 10^{-11}$ (s^{-1})
20	0.1575	0.08857	100	0.1864	0.3966	100	0.2683	2.337
40	0.2364	0.3697	150	0.2311	0.7974	150	0.3104	3.989
60	0.2873	0.7208	200	0.2643	1.267	200	0.3411	5.719
80	0.3242	1.098	250	0.2903	1.793	230	0.3563	6.783

FIG. 1. Thermoelastic stress distributions obtained using the IT_{IM} method, Hugoniot curves, and Rayleigh lines for: (a) 20, (b) 40, (c) 60, and (d) 80 GPa shocks in 2024 Al.

FIG. 2. Temperature distributions in a steady wave front for 80 GPa shock in 2024 Al obtained using the IT_{IM} method and in inviscid 2024 Al solid obtained using Eq. (17a).

the wave fronts (inside temperature distributions) were predicted to a good approximation. The assumption of heat transport was valid and the inside temperature distributions were also predicted fairly accurately for shocks up to 250 GPa in Pt and 230 GPa in Fe.

Temperatures behind the wave fronts T_H for shocks up to 80 GPa in 2024 Al are calculated using the WC equation and the IT_{IM} method and are compared in Table IV. The T_H-V_H distribution obtained using the IT_{IM} method was very close to the correct value obtained using the WC equation, because $\Gamma T/3Nk \ll 1$. In fact, the temperature at 80 GPa was 2374.3 K using the WC equation, while it was 2372.3 K using the IT_{IM} method. For the same reason, both T_H-V_H distributions were fairly close up to 250 GPa in Pt, as compared in Table IV. For 2024 Al and Pt, however, the difference between both temperatures increased a little with shock loading due to ΓT increasing with shock loading. On the other hand, for Fe, both T_H-V_H distributions for any shock loading were completely coincident, because $C_V=3Nk$ was used [see Eq. (11)]. In addition, the $T_H-\sigma_H$ distribution up
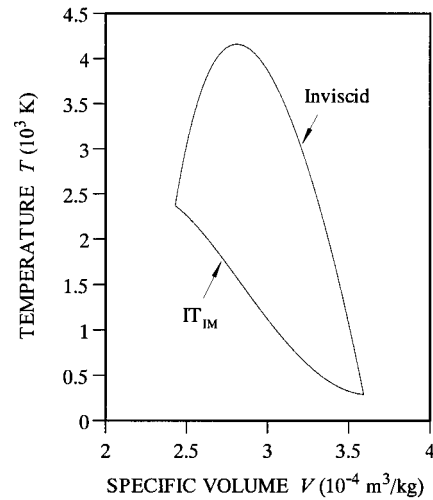
to 230 GPa was consistent with that estimated by Bass *et al.*[5] from their experimental data. These accurate evaluations of the temperatures behind the wave fronts provide further support for the efficacy of the IT_{IM} method.

C. Influence of viscous stress

Figure 2 shows the inside temperature distribution for a 80 GPa shock in an inviscid 2024 Al solid calculated using Eq. (17a). This distribution is convex upward, because Γ decreases monotonically, but thermal stress $(\sigma_T)_{IV}=\sigma-\sigma_C$ decreases and then increases with a decrease in specific volume. Here σ is the stress on the Rayleigh line and subscript IV refers to an inviscid solid. It was much higher than that obtained using the IT_{IM} method, as shown in Fig. 2. The reason for this is accounted for using Eq. (17a).

For an inviscid solid, $\sigma_E=\sigma$, so that $(\sigma_T)_{IV}=\sigma-\sigma_C$ as described above. On the other hand, $\sigma_E=\sigma_{EoS}$ for a solid that is not inviscid, where σ_{EoS} is the stress on the equation-of-state surface of the solid, so that $\sigma_T=\sigma_{EoS}-\sigma_C$. Because σ is not equal to σ_{EoS}, the thermal stresses differ. It follows from $(\sigma_T)_{IV}-\sigma_T=\sigma_v$ that $(\sigma_T)_{IV}>\sigma_T$. Equation (17a) indicates that when thermal stress is large, the temperature is high. Therefore, the higher temperatures for the inviscid 2024 Al solid were due to the viscous stress included in the calculation of temperature. Figures 1(a)–1(d) show that the viscous-stress component for any shock was sufficiently

TABLE IV. Temperatures behind steady wave fronts for 20, 40, 60, and 80 GPa shocks in 2024 Al, for 100, 150, 200, and 250 GPa shocks in Pt, and for 100, 150, 200, and 230 GPa shocks in Fe obtained using the Walsh–Christian (WC) equation and the IT_{IM} method.

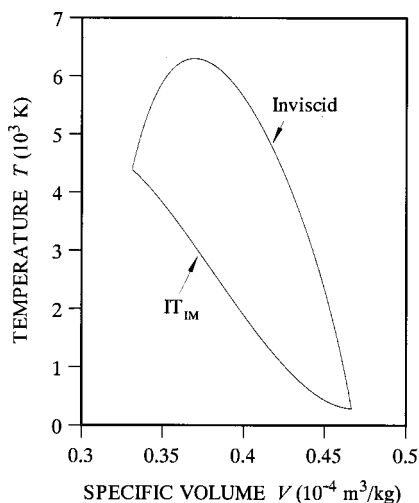| 2024 Al			Pt			Fe		
Shock (GPa)	T_{WC} (K)	T_{IM} (K)	Shock (GPa)	T_{WC} (K)	T_{IM} (K)	Shock (GPa)	T_{WC} (K)	T_{IM} (K)
20	500.77	500.77	100	1138.5	1138.5	100	1948.2	1948.2
40	933.80	933.72	150	2047.5	2045.7	150	3467.9	3467.9
60	1575.4	1574.8	200	3162.7	3155.8	200	5258.2	5258.2
80	2374.3	2372.3	250	4411.3	4394.7	230	6434.4	6434.4

FIG. 3. Temperature distributions in a steady wave front for 250 GPa shock in Pt obtained using the IT_{IM} method and in inviscid Pt solid obtained using Eq. (17a).

large and the viscous-stress component increased with shock loading. As a result, the difference between the temperature distributions in both solids increased with shock loading.

Figure 3 shows inside temperature distributions for the 250 GPa shock in Pt calculated using the IT_{IM} method and Eq. (17a). The higher distribution for an inviscid Pt solid indicates that the viscous-stress components were also great in this case. Both inside temperature distributions in Fig. 4, which were calculated using the IT_{IM} method and Eq. (17b), also indicated that the same was true of the 230 GPa shock in Fe.

IV. MELTING

According to the Kraut–Kennedy rule of melting temperature,[4] which increases in proportion to strain, the melting temperature on the Hugoniot is 2715 K at 88 GPa for 2024 Al and is 5800 K at 304 GPa for Pt.[6] The temperature
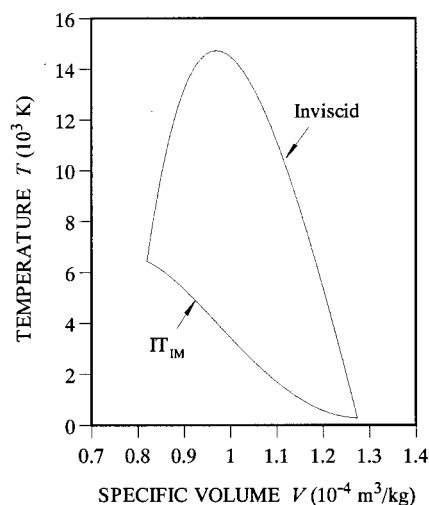

FIG. 4. Temperature distributions in a steady wave front for 230 GPa shock in Fe obtained using the IT_{IM} method and in inviscid Fe solid obtained using Eq. (17b).
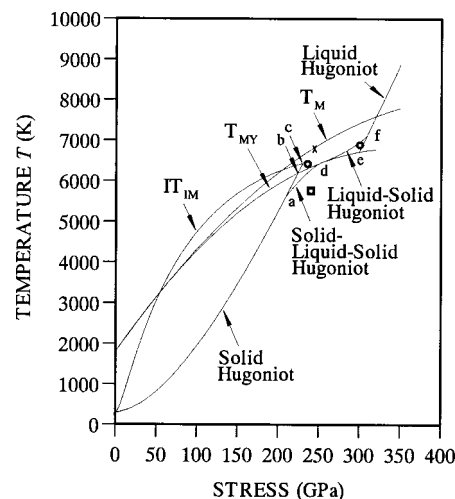

FIG. 5. Solid-Hugoniot temperature ($T_H - \sigma_H$) distribution up to 230 GPa and inside-temperature ($T - \sigma$) distribution for the 230 GPa shock in Fe obtained using the IT_{IM} method, melting-temperature ($T_M - \sigma$) distribution of Fe (see Refs. 5 and 15), new liquid-Hugoniot temperature ($T_H - \sigma_H$) distribution of Fe measured by Yoo et al. (see Ref. 21), and new melting-temperature ($T_{MY} - \sigma$) distribution determined by Yoo et al. using the liquid-Hugoniot temperature distribution. Four experimental data of intermediate states of melting in shock fronts are also shown.

on the Hugoniot for the 80 GPa shock in 2024 Al was sufficiently low compared with the melting temperature. In addition, as shown in Fig. 2, the inside temperature ($T - V$) distribution was below the straight line connecting points (V_0, T_0) and (V_H, T_H) in the range of large specific volume and was near the line in the range of small specific volume. Therefore, this shock was not expected to cause it to melt on the Rayleigh line or in the wave front. The same was true of the 250 GPa shock in Pt.

Many investigators have performed extensive melting studies for Fe, and have advanced both theoretical and experimental aspects of melting temperature–stress relations (for Fe and other metals, see Ahrens and co-workers,[5,11–16] Brown and McQueen,[17] Boehler,[18] Nellis and Yoo,[19] Yoo et al.,[20,21] Saxena et al.,[22] and Duba[23,24]). Figure 5 shows a solid-Hugoniot temperature ($T_H - \sigma_H$) distribution up to 230 GPa and an inside temperature ($T - \sigma$) distribution for the 230 GPa shock in Fe obtained using the IT_{IM} method, together with the melting temperature–stress ($T_M - \sigma$) distribution of Fe (see Fig. 6 in Ref. 5 and Fig. 7 in Ref. 15), a new liquid-Hugoniot temperature ($T_H - \sigma_H$) distribution of Fe measured by Yoo et al., and a new melting-temperature ($T_{MY} - \sigma$) distribution determined using the solid-Hugoniot temperature distribution measured by Yoo et al. and the new liquid-Hugoniot temperature distribution (see Fig. 3 in Ref. 21). The Hugoniot temperature distribution is a locus of end states of temperature and stress (T_H versus σ_H) and the inside temperature distribution is T versus σ through a single shock front (curve labeled IT_{IM}). Point e (300 GPa, 6750 K) on the $T_{MY} - \sigma$ curve is the starting point of the liquid Hugoniot. The solid Hugoniot and the $T_{MY} - \sigma$ curves intersect at point b and the endpoint c of the solid Hugoniot is between both melting curves. Figure 5 also shows some experimental data of intermediate states of melting in shock fronts. The

cross indicates the shock-melting point at 243 GPa (Ref. 5), the box indicates the shock-melting point at 240 GPa (Ref. 17), and the circles indicate the shock-melting points at 235 and 300 GPa (Ref. 20).

Intermediate states of melting in shock fronts are looked for using the $T_{MY}-\sigma$ curve. The $T_{MY}-\sigma$ curve was adapted as the melting curve because this curve was determined using the new solid Hugoniot and liquid Hugoniot as described above, and the transition into a liquid phase from a solid phase in the shock front was assumed to be instantaneous. The $T-\sigma$ curve for the 207 GPa shock contacted with the $T_{MY}-\sigma$ curve at approximately 105 GPa. This means that the solid Hugoniot is up to point a (207 GPa, 5525 K) and curve abc represents no Hugoniot. For a shock beyond point a, the front and rear portions of the wave front might be of solid phases, whereas the middle portion might be of liquid phases. Consequently, the curve from point a to a point on the melting curve between point b and point e might be a solid–liquid–solid Hugoniot. This Hugoniot curve, curve ad, is shown schematically in Fig. 5. Because the temperature rise in a wave portion where solid phases transit into liquid phases is reduced due to the heat of fusion, curve ad is below curve ab. Curve ad is convex upward if the phase transition layer extends with rates increasing with shock loading. For a shock beyond point d, the rear portion of the wave front is of liquid phases. Curve df is a schematic of a liquid–solid Hugoniot. Curve df is concave upward if the phase transition layer extends with rates decreasing with shock loading. It is a difficult problem to theoretically determine point d, point f, and Hugoniot curve adf, even if the phase transition is assumed to be instantaneous.

V. CONCLUSIONS

The temperature distributions in overdriven steady wave fronts for shocks up to 80 GPa in 2024 Al, 250 GPa in Pt, and 230 GPa in Fe were evaluated using the equilibrium thermodynamic theory. Equilibrium thermodynamics are applicable for these shocks, the assumption of heat transport was valid, and the temperatures behind the wave fronts were correct. Thus, the inside temperature distributions were evaluated fairly accurately. The overestimation of the inside temperature distributions in inviscid 2024 Al, Pt, and Fe solids indicated that viscous stress has a large influence on the distributions. Finally, the presence of liquid phases in the wave fronts was examined. A solid–liquid–solid Hugoniot was presented between the solid Hugoniot and liquid–solid Hugoniot for Fe and the solid–liquid–solid and liquid–solid Hugoniots that were a best fit to the experimental data were estimated. We are attempting to develop an equilibrium thermodynamic theory that explicitly includes heat transport, re-examine the applicability of equilibrium thermodynamics, and clarify the dependence of the temperature thickness on the specific volume thickness.

APPENDIX

1. Hugoniot stress

The Hugoniot jump equation for stress is expressed by

$$\sigma_H = \rho_0 U_S U_P, \tag{A1}$$

where U_S is the velocity of a steady wave front and U_P is the particle velocity behind the wave front, which are expressed for 2024 Al and Pt by

$$U_S = c + s U_P, \tag{A2}$$

$$U_P = \frac{c\varepsilon_H}{1 - s\varepsilon_H}, \tag{A3}$$

where $\varepsilon_H = 1 - V_H/V_0$. The values of c and s are listed in Table I. For Fe,

$$U_S = c + s U_P + q U_P^2, \tag{A5}$$

$$U_P = \frac{1 - s\varepsilon_H - \sqrt{1 - 2s\varepsilon_H + (s^2 - 4cq)\varepsilon_H^2}}{2q\varepsilon_H}. \tag{A6}$$

The values of c, s, and q are listed in Table I.

2. Walsh and Christian theory

The thermodynamic equilibrium equation derived by Walsh and Christian[2] is

$$C_V \frac{dT}{dV} + \frac{\gamma_0}{V_0} C_V T = \frac{1}{2} \frac{d\sigma}{dV}(V_0 - V) + \frac{1}{2}(\sigma - \sigma_0), \tag{A7}$$

where C_V, σ, T, and V are the quantities in a Hugoniot state.

[1] Y. Sano and A. Abe, J. Appl. Phys. **89**, 105 (2001).
[2] J. M. Walsh and R. H. Christian, Phys. Rev. **97**, 1544 (1955).
[3] D. C. Wallace, in *Shock Compression of Condensed Matter-1985*, edited by Y. M. Gupta (Elsevier, New York, 1986), p. 37.
[4] E. A. Kraut and G. C. Kennedy, Phys. Rev. **151**, 668 (1966).
[5] J. D. Bass, B. Svendsen, and T. J. Ahrens, in *High-Pressure Research in Mineral Physics*, edited by M. H. Manghnani and Y. Syono (Terra Scientific, Tokyo, 1987), p. 393.
[6] D. C. Wallace, Phys. Rev. B **24**, 5597 (1981); **24**, 5607 (1981).
[7] Ya. B. Zel'dovich and Yu. P. Raizer, in *Physics of Shock Waves and High-Temperature Hydrodynamic Phenomena*, edited by W. D. Hayes and R. F. Probstein (Academic, Orlando, FL, 1966).
[8] L. Davison, J. Appl. Phys. **42**, 5503 (1971).
[9] D. C. Wallace, Phys. Rev. B **22**, 1477 (1980).
[10] R. G. McQueen, S. P. Marsh, J. W. Taylor, J. N. Fritz, and W. J. Crater, in *High Velocity Impact Phenomena*, edited by R. Kinslow (Academic, New York, 1970), p. 293.
[11] Q. Williams, R. Jeanloz, J. Bass, B. Svendsen, and T. J. Aherns, Science **236**, 181 (1987).
[12] B. Svendsen, T. J. Ahrens, and J. D. Bass, in *High-Pressure Research in Mineral Physics*, edited by M. H. Manghnani and Y. Syono (Terra Scientific, Tokyo, 1987), p. 403.
[13] T. J. Ahrens, H. Tan, and J. D. Bass, High Press. Res. **2**, 145 (1990).
[14] H. Tan and T. J. Ahrens, High Press. Res. **2**, 159 (1990).
[15] T. D. Bass, T. J. Ahrens, J. R. Abelson, and T. Hua, J. Geophys. Res. **21**, 776 (1990).
[16] K. G. Gallagher, J. D. Bass, T. J. Ahrens, M. Fitzner, and J. R. Abelson, in *High-Pressure Science and Technology-1993*, edited by S. C. Schmidt, J. W. Shaner, G. A. Samara, and M. Ross (Elsevier, New York, 1994), p. 963.
[17] J. M. Brown and R. G. McQueen, J. Geophys. Res. **91**, 7485 (1986).
[18] R. Boehler, Geophys. Res. Lett. **13**, 1153 (1986).
[19] W. J. Nellis and C. S. Yoo, J. Geophys. Res. **95**, 21749 (1990).
[20] C. S. Yoo, N. C. Holmes, M. Ross, D. J. Webb, and C. Pike, Phys. Rev. Lett. **70**, 3931 (1990).

[21] C. S. Yoo, N. C. Holmes, M. Ross, and E. See, in *High-Pressure Science and Technology-1993*, edited by S. C. Schmidt, J. W. Shaner, G. A. Samara, and M. Ross (Elsevier, New York, 1994), p. 959.

[22] S. K. Saxena, G. Shen, and P. Lazor, Science **260**, 1312 (1993).

[23] A. G. Duba, Nature (London) **359**, 198 (1992).

[24] A. G. Duba, in *High-Pressure Science and Technology-1993*, edited by S. C. Schmidt, J. W. Shaner, G. A. Samara, and M. Ross (Elsevier, New York, 1994), p. 923.